

# Magnetization dynamics of coupled ferromagnetic disks

Olle Heinonen

*Materials Science Division, Argonne National Laboratory, Lemont, Illinois 60439, USA  
and Northwestern-Argonne Institute for Science and Engineering, Evanston, Illinois 60208, USA*

(Received 6 May 2015; revised manuscript received 25 June 2015; published 10 August 2015)

The magnetization configuration in two stacked micron-size ferromagnetic disks can assume different equilibrium states depending on the interfacial coupling between the disks. Here I examine the magnetization dynamics in response to an out-of-plane field pulse for different equilibrium states. For antiferromagnetic coupling, the response spectrum generally consists of a lower-frequency part and a higher-frequency part. The former is related to the response of the core region, which has a significant in-plane response coupled to the out-of-plane one; the latter is related to spin waves generated at the edges of the disk. For a meron structure the response in the two disks to an out-of-plane pulse is also asymmetric.

DOI: [10.1103/PhysRevB.92.054420](https://doi.org/10.1103/PhysRevB.92.054420)

PACS number(s): 76.50.+g, 75.75.Jn, 75.78.Cd

## I. INTRODUCTION

Patterned magnetic nanostructures are fascinating nanoscale laboratories for exploring different and competing interactions by varying geometry and compositions of the structures. This allows for tailoring interactions with the result that new, sometimes unexpected, magnetic structures emerge with interesting properties. One example are artificial spin ices [1], in which geometry is utilized to arrange for competing interactions between individual magnetic nanostructures. Artificial spin ices have been shown to support topological defects [1–3], so-called Dirac monopoles, and Dirac strings [4] that play important roles in the static and quasistatic behavior of the systems [5–11], and also give rise to specific signatures in the resonant spectrum [12]. Another deceptively simple system are two stacked ferromagnetic disks of a diameter of the order of  $1\ \mu\text{m}$  and a few tens of nanometers thick made from a soft magnetic material, such as permalloy (Py). Such single disks have a magnetic vortex configuration as ground state [13–15], which has been explored extensively, both in terms of the static and dynamic properties of the vortex state [16–21]. By stacking the disks on top of one another, the interaction between the disks can be tailored by the materials or thickness of the spacer layer from ferromagnetic to antiferromagnetic. In addition, such systems usually also have a biquadratic coupling between the ferromagnetic layers [22–24]. The static configurations and susceptibility of ferromagnetically and antiferromagnetically arranged vortices in magnetostatically coupled stacked disks were studied by Buchanan *et al.* [25]. Stacked disks have recently been shown to support different equilibrium magnetization structures depending on the coupling between the disks. For soft ferromagnetic disks and ferromagnetic coupling, the magnetization in the disks quite naturally is arranged in two vortices with the same sense of orientation, or chirality, and the same direction of the out-of-plane magnetization at the core (polarity). More surprisingly, a weakly antiferromagnetic coupling can lead to two antiferromagnetically arranged meron structures in the disks [26], the stability of which is further enhanced by biquadratic coupling between the disks [24]. In this arrangement the magnetization is out-of-plane at the center of the disks, just as for a vortex, and then radially outward in one disk, and inward in the other disk, except for near the edges, where the

magnetization is arranged to close flux lines [6]. In fact, this two-meron structure can be obtained by smoothly deforming two ferromagnetically arranged vortices as both structures have the same topological charge. There is, however, a finite energy barrier, related to the magnetization texture on the edges of the disks, for deforming the structure further to obtain two antiferromagnetically arranged vortices. For a larger antiferromagnetic coupling, the ground state of the system is of course two antiferromagnetically arranged vortices.

Given the fact that relatively minor changes in the interlayer coupling between the disks can lead to very different equilibrium states, one would expect concomitantly different low-lying excitation spectra of the magnetization dynamics, since the potential energy for deviations about an equilibrium state depends very much on the state. For example, in single disks, the in-plane dynamics of a skyrmion structure is radically different than that of a vortex [27–30]. The purpose of the work presented here is to explore the magnetization dynamics of stacked soft ferromagnetic disks systems and the experimental consequences. To be precise, I will present detailed micromagnetic simulations of the magnetization dynamics in response to an out-of-plane field pulse, and I will also discuss the response to an in-plane pulse for antiferromagnetically arranged vortices and merons. The resulting response is in the frequency range of a few hundred MHz to a few GHz, and should be relatively easily accessible to experimental techniques, such as time-resolved MOKE [31], PEEMS [32], or broadband meander stripline absorption [33]. In general, one would expect from perturbation theory that two weakly coupled systems (in this case the ferromagnetic disks) will exhibit fundamental modes that are symmetric and antisymmetric combinations of the fundamental modes of the individual systems. As I will show below, this is more or less the case for the ferromagnetically coupled disks, where a low-frequency mode appears, well below the fundamental Kittel-like mode of the system. One would similarly naively expect the modes of antiferromagnetically coupled vortices to be described by perturbation theory, with a low-frequency antisymmetric mode and a high-frequency Kittel-like mode. This is however not the case. The spectrum of modes for this system is fundamentally different from the spectrum of an individual vortex and not readily obtainable from those of the individual vortices. Instead, the spectrum of modes

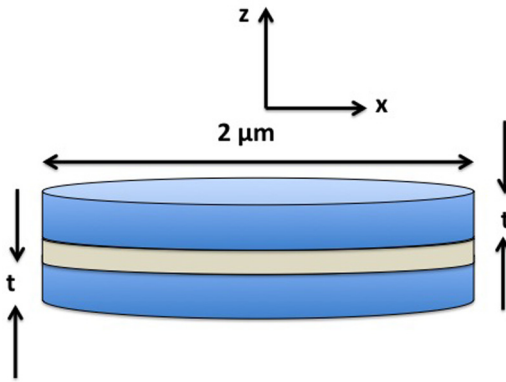


FIG. 1. (Color online) Cartoon of the stacked disks considered here. The spacer is a thin metal that can promote ferromagnetic or antiferromagnetic and biquadratic coupling between the disks.

responding to the out-of-plane pulse is much more complicated with distinct low-frequency parts, corresponding to resonant modes localized near the core region, and high-frequency parts, corresponding to spin waves. Finally, for a system in an initial configuration with antiparallel merons (with or without biquadratic coupling), the low-frequency response is also strongly asymmetric (neither symmetric nor antisymmetric) in the two disks.

The systems considered here consist of two Py disks of a diameter of  $2 \mu\text{m}$  and a thickness of  $t$  nm (Fig. 1). Typically  $t$  was taken to be 10 nm, except for the ferromagnetically coupled disks, for which  $t$  was 20 nm. The disks are stacked with a spacer layer of negligible thickness but that can promote an interfacial coupling that is either weakly ferromagnetic or weakly antiferromagnetic with or without a biquadratic coupling. The equilibrium states for these three interactions are ferromagnetic vortices, antiferromagnetic vortices, or antiferromagnetic meron structures.

The system is subjected to an out-of-plane magnetic pulse of duration of some fraction of a nanosecond and of strength of a few tens to 100 Oe. The dynamical magnetization response is then obtained by integrating the Landau-Lifshitz-Gilbert equation

$$\frac{d\hat{m}}{dt} = -|\gamma_e|\hat{m} \times \mathbf{H}_{\text{eff}} - \frac{|\gamma_e|\alpha}{1+\alpha^2}\hat{m} \times [\hat{m} \times \mathbf{H}_{\text{eff}}]. \quad (1)$$

Here  $\hat{m}$  is the local magnetization director of unit norm,  $|\gamma_e|$  is the electron gyromagnetic ratio, and  $\mathbf{H}_{\text{eff}}$  is the effective magnetic field that includes micromagnetic exchange, interfacial coupling, external field, and magnetostatic fields. In the simulations presented here, the magnetostatic field was calculated at each time step using a fast Fourier technique and a mesh of size  $2.5 \text{ nm} \times 2.5 \text{ nm} \times 5 \text{ nm}$ , and the time integration was done using a modified Bulirsch-Stoer implicit integrator [34] in time steps ranging from 0.25 to 1 ps. This mesh was necessary for the antiferromagnetically coupled disks. A coarser mesh ( $5 \text{ nm} \times 5 \text{ nm} \times 5 \text{ nm}$ ) for these systems gave one-dimensional (1D) spectra in good quantitative agreement with the finer mesh, but the two-dimensional (2D) images of the magnetization modes for antiferromagnetic coupling were typically distorted at the lower frequencies with a twofold or fourfold symmetry originating from magnetization errors

due to the “staircase” approximation of the circumference. For the ferromagnetically coupled disks coarser mesh of dimensions  $5 \text{ nm} \times 5 \text{ nm} \times 5 \text{ nm}$  was adequate. The materials parameters used, typical for permalloy, were a saturation magnetization  $M_S = 800 \text{ emu/cm}^3$  and a dimensionless damping ranging from  $\alpha = 0.01$  to 0.02, and an exchange coupling of  $1.2 \mu\text{erg/cm}$ . The interfacial coupling was typically of magnitude  $0.015 \text{ erg/cm}^2$ , translating to an effective field of magnitude 18 Oe throughout the thickness of each disk [7], and the biquadratic coupling field was 15 Oe. The time-integrated magnetization density was sampled every 25 ps for a duration of 10 ns, and this time sequence of magnetization was then Fourier transformed to give spatial magnetization structure as a function of frequency. The average magnetization in each layer was also collected every 25 ps and Fourier transformed to yield 1D plots of each average magnetization component as a function of frequency.

## II. RESULTS AND DISCUSSION

### A. Response to out-of-plane field pulse

Figure 2 depicts the spectrum of the out-of-plane magnetization for the two disks for the case of two ferromagnetically coupled vortices. Here the disks were 20 nm thick and the interlayer exchange coupling varying between 0.01 and  $0.1 \text{ erg/cm}^2$ . The spectrum shows one high-amplitude peak close to 7 GHz, which corresponds to a nodeless circularly symmetric out-of-plane motion of the magnetization. In addition to this main resonance, Fig. 2 shows smaller peaks at about 11 and 13 GHz, corresponding to high-order circularly symmetric resonances with one and two nodal lines in the radial direction. The frequencies of these circularly symmetric radial modes are in very good agreement with the results of Guslienko *et al.* [35], who calculated these modes for a single

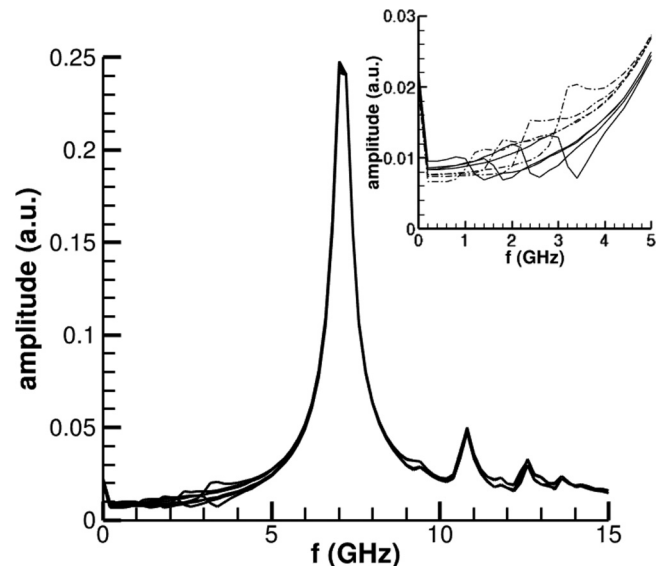


FIG. 2. Spectrum of the out-of-plane magnetization for ferromagnetically coupled disks with interlayer coupling of 0.01, 0.025, 0.05, and  $0.1 \text{ erg/cm}^2$ . The inset shows the region of the low-frequency mode with dash-dotted (solid) lines the amplitude of the upper (lower) disk. The frequency increases with increasing interlayer coupling.

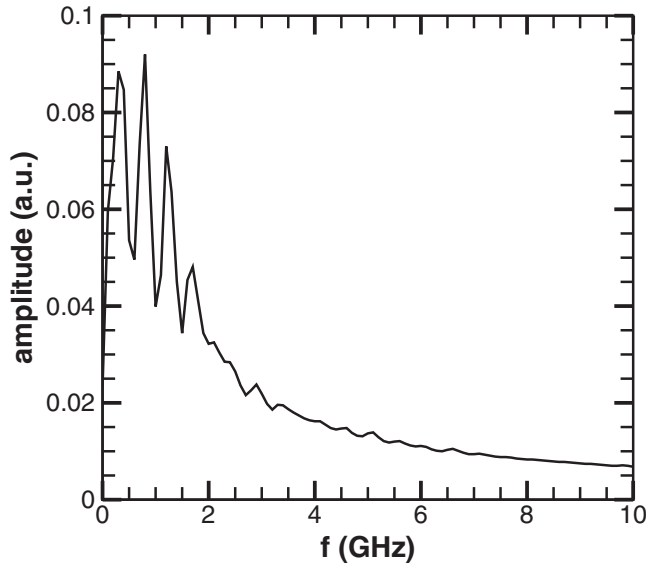


FIG. 3. Magnetization spectrum for the out-of-plane magnetization component for two antiferromagnetic vortices.

disk using analytical and micromagnetic techniques, if the two stacked disks are considered as a single disk of total thickness 40 nm. For all these high-frequency modes, the amplitude is identical in the two disks. The inset of Fig. 2 shows an enlargement of the low-frequency region. The peaks here, increasing in frequency with increasing interlayer coupling, are the lower-frequency asymmetric mode that arises because of the coupling. A simple model [36] yields frequencies of about 2 GHz for this lower mode, which is in good agreement with the micromagnetic simulations. Strictly speaking, this mode is not perfectly antisymmetric—if it were, it would not couple at all to the out-of-plane magnetic field pulse.

In contrast, the 1D spectrum for the antiferromagnetically aligned vortices (interfacial coupling  $-0.015$  erg/cm<sup>2</sup>, with the sign denoting antiferromagnetic coupling) shows a number of low-frequency peaks in the out-of-plane magnetization (Fig. 3) at about 0.3, 0.8, 1.2, 1.7, 2.1, and 2.9 GHz, in addition to some smaller peaks at higher frequencies. Again, the out-of-plane magnetization motion in the two disks is identical in both amplitude and phase, while the in-plane magnetization motion is opposite in the two disks, as is to be expected. Plots of the out-of-plane magnetization amplitude (Figs. 4 and 5) show that the the lower-frequency modes are located near the core at the center of the disk. As the mode frequency increases, the modes extend more and more outside the core region, and gradually turn into small-wavelength spin waves [36]. The applied out-of-plane field pulse causes an in-plane clockwise screw distortion of both the initial vortices, together with an out-of-plane component of the magnetization (see Fig. 6). This screw distortion is caused by antiparallel radial (and parallel out-of-plane) magnetization distortions in the two disks. After the application of the out-of-plane pulse, the magnetization in the two disks starts to relax. The relaxation of the screw distortion takes place through a combination of slow out-of-plane magnetization motion coupled to in-plane motion. This gives rise to the amplitude distribution near the center of the disks at the lower frequencies

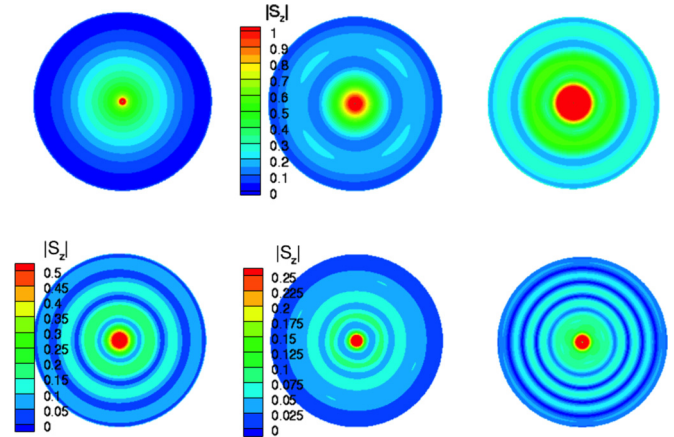


FIG. 4. (Color online) Amplitude of the out-of-plane magnetization for antiferromagnetically coupled vortices from top left to bottom right: 0.3, 0.8, 1.2, 1.7, 2.1, and 2.9 GHz. The color scale shows amplitude in arbitrary units. Top two rows use the same color scale shown on the center panel; the bottom row uses a different color scale (as the amplitude is lower in these modes) for the bottom left panel, and yet another one for the center and right bottom panels.

$\lesssim 2.0$  GHz. At the edge of the disk, the relaxation occurs with an out-of-plane motion (the magnetization is “flapping” at the edge) that generates circularly symmetric spin waves that propagate inward and give rise to the approximately circularly symmetric amplitude distributions at  $\gtrsim 2.0$  GHz.

For the meron structure with an antiferromagnetic interfacial coupling of  $-0.015$  erg/cm<sup>2</sup>, the 1D out-of-plane spectrum shows some different, interesting features (Fig. 7). The out-of-plane magnetization in both disks has a peak at 0.4 and about 1.1 GHz, but with one disk (the top disk) a larger amplitude, especially at about 1.1 GHz. The top disk amplitude also has a peak at about 1.9 GHz, but the magnetization amplitude in the other disk shows a *dip* at this frequency (Fig. 7). The amplitude in both disks have a number of smaller peaks at higher frequencies. Two-dimensional representations of the out-of-plane magnetization amplitude show that the two lowest-frequency modes are somewhat similar to the low-frequency mode of the antiferromagnetic vortices with

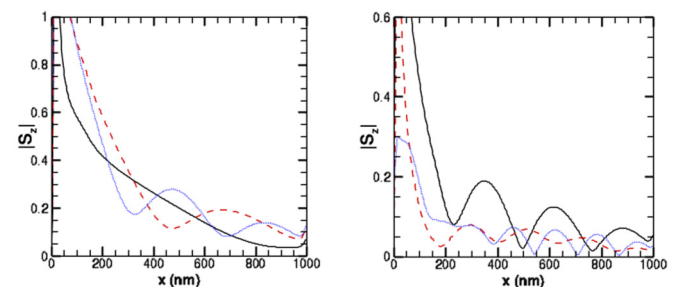


FIG. 5. (Color online) Plot of the amplitude of the  $z$  component of the magnetization eigenmodes in Fig. 4 as a function of radius  $r$  from the center of the disk. Left panel: 0.3 GHz (black solid line), 0.8 GHz (red dashed line), and 1.2 GHz (blue dotted line). Right panel: 1.7 GHz (black solid line), 2.1 GHz (red dashed line), and 2.9 GHz (blue dotted line). Note that the nodes in the amplitude do not go strictly to zero because of numerical noise.

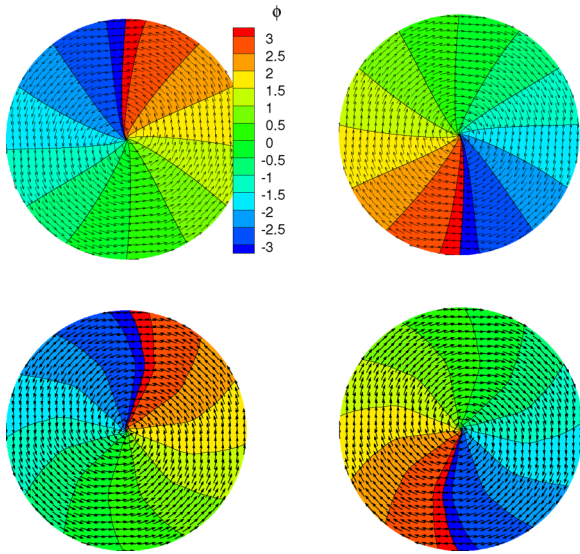


FIG. 6. (Color online) Equilibrium magnetization (top row) and initial magnetization configuration of the antiparallel vortices (bottom row) in the bottom (left panels) and top (right panels) disks after the application of a 500 ps out-of-plane field of magnitude 100 Oe. The color scales shows the azimuthal angle in radians, and the arrows depict the in-plane magnetization.

the high amplitude in a region about the center (Figs. 8 and 9). The mode with a peak at about 2.0 GHz, on the other hand, has a weak amplitude maximum in a band approximately at half the disk radius in the bottom disk, while the top disk has a strong maximum at 1.9 GHz in the same band. Examination of the magnetization dynamics shows that the magnetization at the edges now does not respond much at all to the pulse. This is because for the meron configuration, the equilibrium magnetization goes largely out-of-plane at the edges of the disks to close flux between the disks. This out-of-plane magnetization leads to a much smaller response to an external

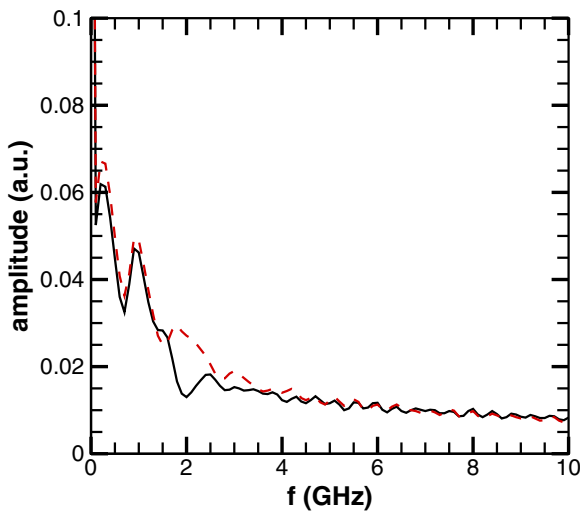


FIG. 7. (Color online) Magnetization spectrum for the out-of-plane magnetization components in the two disks for a meron configuration (bottom disk: solid black line, top disk: dot-dashed red line) for a meron structure.

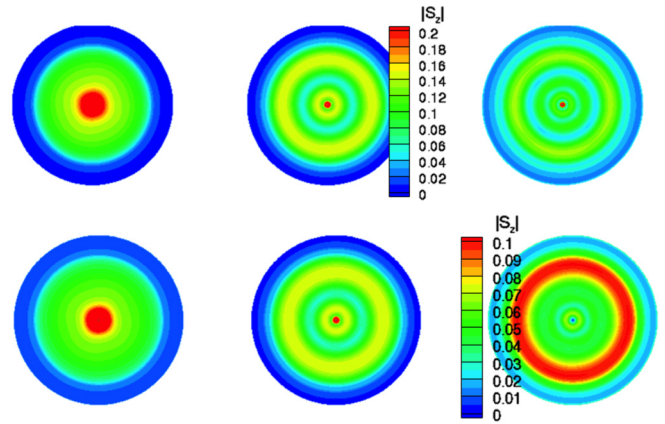


FIG. 8. (Color online) 2D representation of the out-of-plane magnetization motion in the two disks for a meron configuration; top row shows the bottom disk at 0.3, 1.0, and 2.0 GHz; bottom row shows the top disk at 0.3, 1.0, and 2.0 GHz.

magnetic field, and as the magnetization relaxes, there is no “large-amplitude edge-flapping” as for the antiferromagnetic vortices, but there are in this case too spin waves that are generated at the edge and propagate inwards. This results in the smaller peaks at frequencies  $\gtrsim 2.5$  GHz. The antiferromagnetic coupling again leads to an in-plane response that is opposite in the two disks near the core. The magnetization in the disks responds in the core region to the initial out-of-plane field pulse by screw distortions of the magnetization together with increasing the out-of-plane magnetization (see Fig. 10), similar to the AP vortices. In contrast with the initial distortion of the AP vortices that were both distorted equally in a clockwise sense, for the meron structure the magnetization in the bottom is distorted differently than that of the top disk, with a resulting different relaxation dynamics. The response to the initial pulse near the edge also has an in-plane component, but much less pronounced than in the interior of the disks. The in-plane components relax in two stages, faster in the outer region of the disk, and much more slowly in the core region. The faster relaxation in the outer region is strongly suppressed in amplitude in a band at about half the radius from the center, and this results in the dip of the out-of-plane spectrum at about

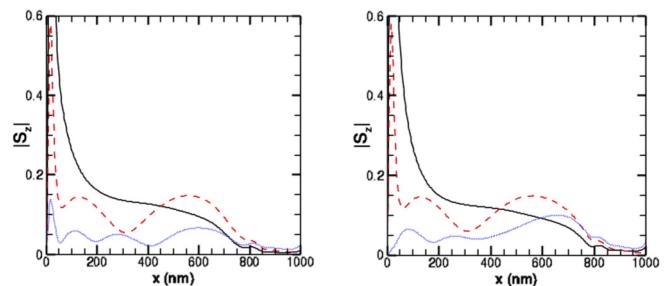


FIG. 9. (Color online) Plot of the amplitude of the  $z$  component of the meron magnetization eigenmodes in Fig. 8 as a function of radius  $r$  from the center of the disk. Left panel bottom disk, right panel top disk, 0.3 GHz (solid black line), 1.0 GHz (red dashed line), and 2.0 GHz (blue dotted line). Note that the nodes in the amplitude do not go strictly to zero because of numerical noise.

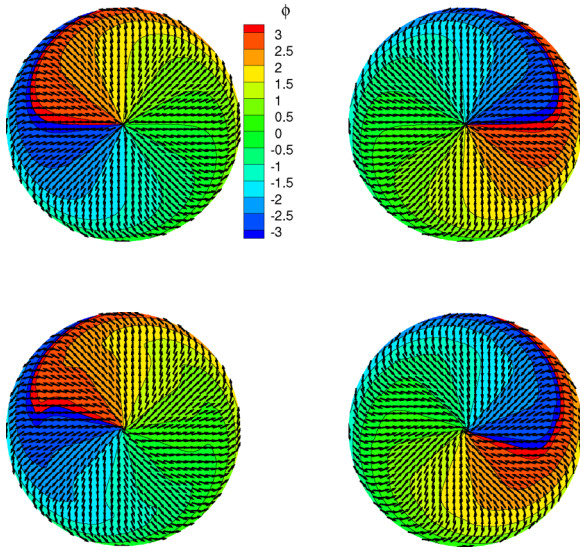


FIG. 10. (Color online) 2D representation of the equilibrium (top row) and initial magnetization at the end of the out-of-plane magnetization pulse (bottom row) in the bottom (left panels) and top (right panels) disks for the meron structure. The arrows depict the in-plane magnetization, which is approximately radially inward in the bottom disk (left panel) and radially outward in the top disk (right panel); the color coding depicts azimuthal angle of the local magnetization density.

2.0 GHz (Fig. 7). The slower relaxation in the core unwinds the screw displacements in the two disks, giving rise to the larger spectral feature at 0.3 and 1.0 GHz.

I note that simulations were also performed for the two-meron structure with initial opposite core polarizations. However, the meron cores are rather soft and the field pulse reversed the core polarization in one disk, at least for the field pulse used here (100 Oe), resulting in same-polarity structures.

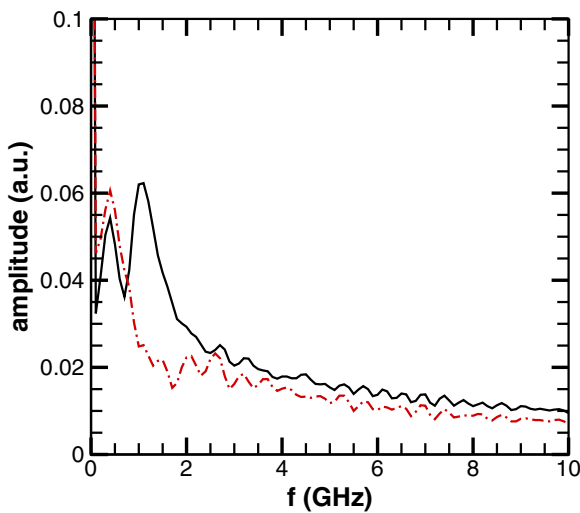


FIG. 11. (Color online) Magnetization dynamics spectrum for the out-of-plane magnetization in the two disks (top layer: solid black line, bottom layer: red dash-dotted line) with an antiferromagnetic interlayer coupling of  $-0.015$  erg/cm<sup>2</sup> and a biquadratic coupling of 15 Oe; the disk ground state configuration is antiparallel merons.

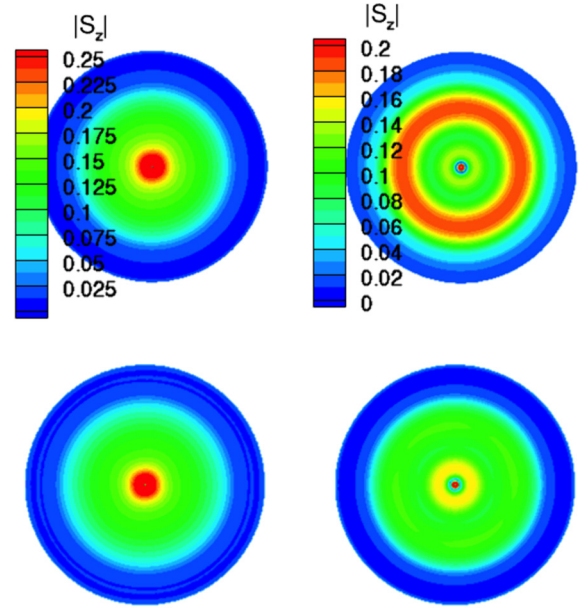


FIG. 12. (Color online) 2D magnetization modes at 0.4 GHz (left panels) and 1.1 GHz (right panels) for bottom and top layers of the meron system with added biquadratic coupling.

Finally, Fig. 11 shows the out-of-plane spectrum for the meron structure with now and added biquadratic coupling. There are two larger peaks at 0.4 and 1.1 GHz, and some smaller and broader peaks above 2.0 GHz (Fig. 11). The lower mode at 0.4 GHz is a mode with its amplitude in a broad range centered on the core, while the 1.1 GHz mode is similar to the asymmetric mode for merons with purely antiferromagnetic coupling: There is a band of high amplitude at about half the radius in one disk, while the amplitude is much suppressed in the other disk (Fig. 12).

**B. Response to in-plane field pulse**

The response to an in-plane field pulse by a single vortex or magnetostatically coupled stacked vortices have been studied extensively [16–21,37]. It is well known that a single vortex displays a gyrotropic motion in which the initially laterally displaced core spirals back to its equilibrium position. The direction of rotation depends only on the core polarity and not on the chirality of the vortex. For same polarities of the

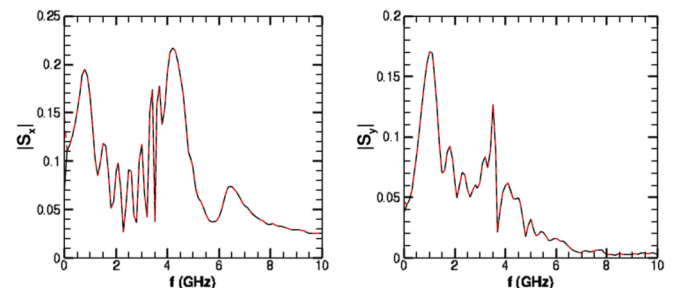


FIG. 13. (Color online) Magnetization spectra of the x components (left panel) and y component (right panel) of the magnetization in two antiferromagnetically aligned vortices after an in-plane field pulse along the x axis.

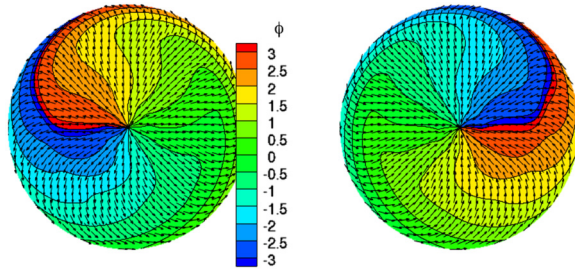


FIG. 14. (Color online) Magnetization configuration in the anti-ferromagnetically coupled meron structures after a 0.5 ns field pulse of magnitude 20 Oe along the  $x$  axis. The color coding represents the azimuthal angle of the local magnetization density in the bottom (right panel) and top (left panel) disks. Note that the cores of the merons have not been displaced laterally.

core, there are two fundamental modes corresponding to spiral motions of the cores and a low-frequency rotation of the mean core position [37].

Figure 13 shows the spectra of the  $x$  and  $y$  components of the magnetization of the anti-ferromagnetically coupled vortices studied here after a 0.5 ns pulse of 20 Oe along the  $x$  direction for same core polarities. The lowest peak at about 0.75 GHz does indeed correspond to the vortex cores spiraling back towards the center, with the cores approximately on opposite sides of the disk center. The higher-frequency peaks appear to correspond to much more complicated dynamics with higher harmonics of the core motions coupled to spin waves with nodes in the azimuthal directions.

In contrast, the two-meron structure does *not* respond to an in-plane pulse by displacing the cores laterally from the center. Instead, the response to the pulse is first to distort the magnetization in the two disks to increase the magnetization along the field, and decrease the magnetization antiparallel to the field; this initial distortion is antisymmetric in the two disks (see Fig. 14). The restoring dynamics mostly consists of a slight in-plane rotation of the magnetization about its equilibrium. Figure 15 shows the spectra of the in-plane magnetization motion for the two disks. The main features are the peaks at about 0.4, 1, and 2.0 GHz. The corresponding 2D representations of the dynamic  $y$  component is shown in Fig. 16 for the two disks. Again, the motions appear rather complicated, but at the lowest frequency (leftmost panel) the

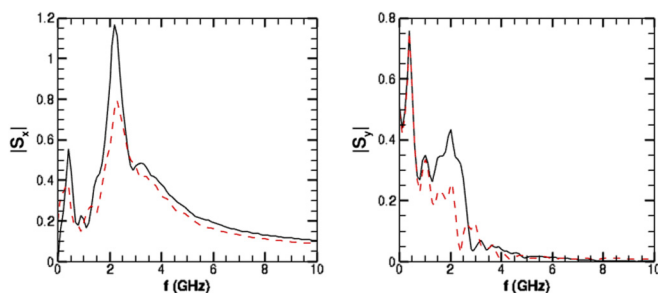


FIG. 15. (Color online) Magnetization spectra of the  $x$  components (left panel) and  $y$  components of the magnetization in the two-meron structure after an in-plane field pulse along the  $x$  axis. The solid line is for the bottom disk, and the dashed (red) line for the top disk.

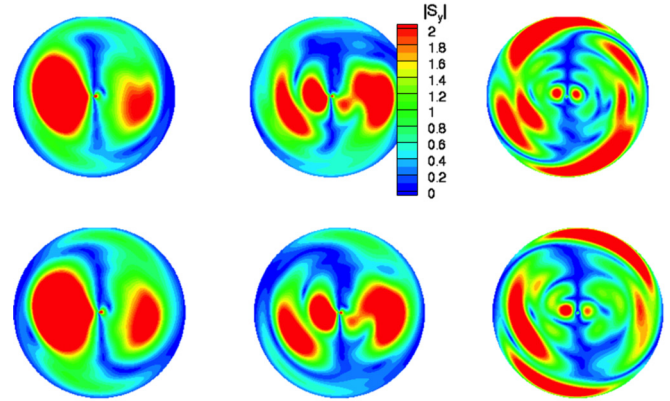


FIG. 16. (Color online) 2D magnetization modes ( $y$  components) of the meron structure after an in-plane field pulse along the  $x$  axis at 0.4, 1.0, and 2.0 GHz from left to right; the top (bottom) row shows the amplitude for the bottom (top) disk.

amplitude is high in two lobes on opposite sides of the center along the  $x$  axis; these correspond to the  $y$  component of the slow restoring rotation. The dynamics at about 1 GHz correspond to a higher harmonic of this motion, while at 2.0 GHz the dynamics is more along the edge. Note again that the response in the two disks is not the same, similar to the response to the out-of-plane field pulse.

### III. CONCLUSIONS

Very slight changes in the interlayer coupling between the ferromagnetic disk can lead to very different ground states or equilibrium magnetic configurations. This completely alters the energy landscape for the dynamics of eigenmodes with remarkably different responses to external field pulses as a consequence, both in terms of the frequency content of the response as well as the spatial distribution of the magnetization dynamics. Therefore, these systems are convenient laboratories for exploring how competing interactions can give very large changes in the system behavior as a result of small changes in a control parameter. The response for ferromagnetically coupled vortices can be readily understood from simple mode-coupling theory in the weak coupling regime, with a Kittel-like nearly uniform (symmetric) mode, in this case near 7 GHz, and an additional lower-frequency nearly antisymmetric mode. In contrast, the response of anti-ferromagnetically coupled vortices or meronlike structure is dominated by low-frequency modes around 1 GHz resulting from the relaxation of an initial screw distortion of the magnetization from its equilibrium configuration. In addition, for the anti-ferromagnetic coupling, there is a large response at or near the edge of the disks, resulting in the generation of circularly symmetric spin waves that propagate inward. In the absence of biquadratic coupling, the meron structure shows a frequency response that is different in the two disks, with one disk exhibiting a response at about 1.9 GHz; the amplitude has a pronounced *minimum* in the other disk. For this system, the symmetry of the modes of the system are broken between the disks. The response modes of disks with added biquadratic coupling show similar behavior.

The frequencies ranges explored here are experimentally accessible so the results presented here can be verified experimentally. They also provide new avenues to explore—with potentially interesting and useful applications—the dynamics of coupled magnetic nanostructures. The results presented here should also be useful in the context of designing and interpreting experiments exploring spin-transfer torque induced magnetization dynamics in nanopillars with diameters large enough to support vortex or meron structures [38,39].

## ACKNOWLEDGMENTS

This work was supported by the Department of Energy, Office of Science, Materials Science and Engineering Division. I gratefully acknowledge the computing resources provided on Blues, a high-performance computing cluster operated by the Laboratory Computing Resource Center at Argonne National Laboratory.

- 
- [1] R. F. Wang, C. Nisoli, R. S. Freitas, J. Li, W. McConville, B. J. Cooley, M. S. Lund, N. Samarth, C. Leighton, V. H. Crespi, and P. Schiffer, *Nature (London)* **439**, 303 (2006).
- [2] S. Ladak, D. E. Read, G. K. Perkins, L. F. Cohen, and W. R. Branford, *Nat. Phys.* **6**, 359 (2010).
- [3] E. Mengotti, L. J. Heyderman, A. F. Rodriguez, F. Nolting, R. V. Hugli, and H.-B. Braun, *Nat. Phys.* **7**, 68 (2011).
- [4] M. J. P. Gingras, *Science* **326**, 375 (2009).
- [5] J. P. Morgan, A. Stein, S. Langridge, and C. H. Marrows, *Nat. Phys.* **7**, 75 (2011).
- [6] C. Phatak, A. K. Petford-Long, O. Heinonen, M. Tanase, and M. De Graef, *Phys. Rev. B* **83**, 174431 (2011).
- [7] C. Phatak, M. Pan, A. K. Petford-Long, S. Hong, and M. De Graef, *New J. Phys.* **14**, 075028 (2012).
- [8] A. Westphalen, A. Schumann, A. Remhof, H. Zabel, M. Karolak, B. Baxevanis, E. Y. Vedmedenko, T. Last, U. Kunze, and T. Eimüller, *Phys. Rev. B* **77**, 174407 (2008).
- [9] V. Kapaklis, U. B. Arnalds, A. Harman-Clarke, E. T. Papaioannou, M. Karimipour, P. Kerelis, A. Taroni, P. C. W. Holdsworth, S. T. Bramwell, and B. Hjörvarsson, *New J. Phys.* **14**, 035009 (2012).
- [10] Y. Shen, O. Petrova, P. Mellado, S. Dauheimer, J. Cumings, and O. Tchernyshyov, *New J. Phys.* **14**, 035022 (2012).
- [11] Z. Budrikis, K. L. Livesey, J. P. Morgan, J. Åkerman, A. Stein, S. Langridge, C. H. Marrows, and R. L. Stamps, *New J. Phys.* **14**, 035014 (2012).
- [12] S. Gliga, A. Kákay, R. Hertel, and O. G. Heinonen, *Phys. Rev. Lett.* **110**, 117205 (2013).
- [13] S. Choi, K.-S. Lee, K. Y. Guslienko, and S.-K. Kim, *Phys. Rev. Lett.* **98**, 087205 (2007).
- [14] B. V. Waeyenberge, A. Puzic, H. Stoll, K. W. Chou, T. Tylliszczak, R. Hertel, M. Fahnle, H. Bruckl, K. Rott, G. Reiss, I. Neudecker, D. Weiss, C. H. Back, and G. Schutz, *Nature (London)* **444**, 461 (2006).
- [15] S.-K. Kim, K.-S. Lee, Y.-S. Yu, and Y.-S. Choi, *Appl. Phys. Lett.* **92**, 022509 (2008).
- [16] K. Y. Guslienko, B. A. Ivanov, V. Novosad, Y. Otani, H. Shima, and K. Fukamichi, *J. Appl. Phys.* **91**, 8037 (2002).
- [17] J. P. Park, P. Eames, D. M. Engebretson, J. Berezovsky, and P. A. Crowell, *Phys. Rev. B* **67**, 020403 (2003).
- [18] S. Kasai, Y. Nakatani, K. Kobayashi, H. Kohno, and T. Ono, *Phys. Rev. Lett.* **97**, 107204 (2006).
- [19] V. S. Pribiag, I. N. Krivorotov, G. D. Fuchs, P. M. Braganca, O. Ozatay, J. C. Sankey, D. C. Ralph, and R. A. Buhrman, *Nat. Phys.* **3**, 498 (2007).
- [20] A. Dussaux, B. Georges, J. Grollier, V. Cros, A. V. Khvalkovskiy, A. Fukushima, M. Konoto, H. Kubota, K. Yakushiji, S. Yuasa, K. A. Zvezdin, K. Ando, and A. Fert, *Nat. Commun.* **1**, 8 (2010).
- [21] K.-S. Lee and S.-K. Kim, *Phys. Rev. B* **78**, 014405 (2008).
- [22] J. Unguris, R. J. Celotta, and D. T. Pierce, *Phys. Rev. Lett.* **67**, 140 (1991).
- [23] J. C. Slonczewski, *Phys. Rev. Lett.* **67**, 3172 (1991).
- [24] S. Wintz, C. Bunce, A. Neudert, M. Körner, T. Strache, M. Buhl, A. Erbe, S. Gemming, J. Raabe, C. Quitmann, and J. Fassbender, *Phys. Rev. Lett.* **110**, 177201 (2013).
- [25] K. S. Buchanan, K. Y. Guslienko, A. Doran, A. Scholl, S. D. Bader, and V. Novosad, *Phys. Rev. B* **72**, 134415 (2005).
- [26] C. Phatak, A. K. Petford-Long, and O. Heinonen, *Phys. Rev. Lett.* **108**, 067205 (2012).
- [27] C. Moutafis, S. Komineas, and J. A. C. Bland, *Phys. Rev. B* **79**, 224429 (2009).
- [28] I. Makhfudz, B. Krüger, and O. Tchernyshyov, *Phys. Rev. Lett.* **109**, 217201 (2012).
- [29] Y. Y. Dai, H. Wang, P. Tao, T. Yang, W. J. Ren, and Z. D. Zhang, *Phys. Rev. B* **88**, 054403 (2013).
- [30] F. Buttner, C. Moutafis, M. Schneider, B. Kruger, C. M. Gunther, J. Geilhufe, C. v Korff Schmising, J. Mohanty, B. Pfau, S. Schaffert, A. Bisig, M. Foerster, T. Schulz, C. A. F. Vaz, J. H. Franken, H. J. M. Swagten, M. Klaui, and S. Eisbett, *Nat. Phys.* **11**, 225 (2015).
- [31] G. Zhang, W. Hübner, G. Lefkidis, Y. Bai, and T. George, *Nat. Phys.* **5**, 499 (2009).
- [32] Y. Hwu, W. Tsai, B. Lai, J. Je, G. Fecher, M. Bertolo, and G. Margaritondo, *Surf. Sci.* **480**, 188 (2001).
- [33] C. C. Tsai, J. Choi, S. Cho, S. J. Lee, B. K. Sarma, C. Thompson, O. Chernyashevskyy, I. Nevirkovets, and J. B. Ketterson, *Rev. Sci. Instrum.* **80**, 023904 (2009).
- [34] O. G. Heinonen, D. K. Schreiber, and A. K. Petford-Long, *Phys. Rev. B* **76**, 144407 (2007).
- [35] K. Y. Guslienko, W. Scholz, R. W. Chantrell, and V. Novosad, *Phys. Rev. B* **71**, 144407 (2005).
- [36] D. K. Schreiber, O. G. Heinonen, and A. K. Petford-Long, *Phys. Rev. B* **80**, 014411 (2009).
- [37] K. Y. Guslienko, K. S. Buchanan, S. D. Bader, and V. Novosad, *Appl. Phys. Lett.* **86**, 223112 (2005).
- [38] K. Y. Guslienko, G. R. Aranda, and J. Gonzales, *J. Phys. Conf. Series* **292**, 012006 (2011).
- [39] V. S. A. Kakay, A. M. Deac, D. E. Burgler, C. M. Schneider, and R. Hertel, *Nat. Commun.* **6**, 6409 (2015).